Passive Flow Control of Mach 4 Mixed-Compression Intake Using Chevron Grooves

Yash A Gujar
AIAE, Amity University Uttar Pardesh Noida
India

Srishti Tyagi
AIAE, Amity University Uttar Pardesh,
Noida,
India

Aafrin S Mehboob
AIAE, Amity University Uttar Pardesh,
Noida,
India

Narender Singh
AIAE, Amity University Uttar Pardesh,
Noida,
India

Rajesh K. Saluja
AIAE, Amity University Uttar Pardesh,
Noida,
India

Manish Naagar
School of Engineering aznd Computing,
Dev Bhoomi Uttarakhand University,
Dehradun, Uttarakhand,
India

Neeraj Kumar Gahlot
AIAE, Amity University Uttar Pardesh,
Noida,
India

Efficient operation of supersonic intakes is frequently hindered by shock–boundary layer interaction (SBLI), which induces large separation bubbles, pressure losses, and non-uniform flow at the engine face. To address these challenges, this work introduces Chevron Groove Modifications (CGM) as a novel passive flow-control strategy. A two-dimensional Mach 4 mixed-compression intake was modeled, and three groove configurations, downward, mid-surface, and upward were implemented on the ramp surface near the shock foot. High-resolution Reynolds-Averaged Navier–Stokes (RANS) simulations with the k–ω SST model were performed to assess the effects on separation factor (SF), total pressure recovery (TPR), and distortion coefficient (DC). Results indicate that upward chevron grooves (Case U-1) provided the most effective control, collapsing the throat separation bubble by approximately 83%, reducing distortion by ~30%, and enhancing TPR compared to the baseline case. Further parametric studies on groove depth and frequency revealed that shallow, high-frequency grooves (Case U-1B: 1 mm depth, frequency = 8) achieved the best balance, yielding smooth pressure distributions, low SF values, and distortion reduced to 38.8%. These improvements are attributed to the generation of strong counter-rotating vortices, which re-energize the boundary layer and weaken adverse shock interactions. Additional three-dimensional simulations confirm the reliability of the 2D predictions and capture spanwise effects. Off-design analyses across Mach 2.5–4.0 demonstrate that CGM enhances intake robustness, maintaining stable supersonic flow while imposing negligible drag penalties.These findings establish chevron grooves as an effective, geometry-based passive control technique to improve stability, pressure recovery, and operability in high-speed air-breathing propulsion systems.

Keywords: *Supersonic intake, Shockboundary layer interaction (SBLI), Chevron groove modification (CGM), Passive flow control, Total pressure recovery (TPR), Flow distortion.*

1. INTRODUCTION

Efficient and stable operation of scramjet engines, the cornerstone of future hypersonic flight, is critically dependent on the performance of the supersonic intake. This component must decelerate and compress vast quantities of supersonic air with minimal loss before it enters the combustor. The key performance parameters of such an intake are the total pressure recovery (TPR) and the mass capture ratio (MCR), which directly affect engine thrust and stability [1].Therefore, careful intake design is essential to avoid problems like flow separation, shock loss, or unstart, which reduce engine efficiency and stability [2]. In a supersonic intake, shock waves are the primary mechanism used to decelerate and compress the high-speed incoming airflow before it enters the engine [3]. When these shocks interact with the boundary layer near the walls, they can trigger shock boundary layer interaction (SBLI), leading to flow separation and loss of pressure recovery [4]. This separation leads to the formation of low-momentum recirculating zones, known as separation bubbles, which thicken the boundary layer and disrupt the smooth progression of airflow [5].

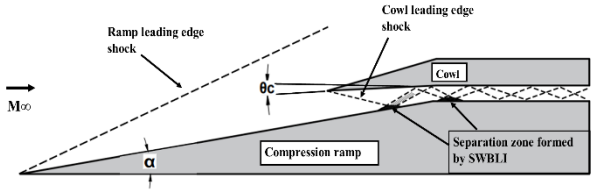

Figure 1. Schematic of a mixed-compression supersonic intake showing ramp and cowl generated shocks, SBLI and the resulting separation zone near the ramp and throat region.

As a result, the downstream flow becomes distorted and uneven. This distorted, low-energy flow at the engine face not only compromises combustion stability

Received: October 2025, Accepted: Decembar 2025
Correspondence to: Neeraj Kumar Ghalot, Amity Institute of Aerospace Engineering (AIAE), Amity University Uttar Pardesh, Noida, India
E-mail: neerajkumargahlot@gmail.com
doi: 10.5937/fme2601053G

and thrust but can also trigger catastrophic events like engine unstart [6,7], leading to a complete loss of propulsion. Figure 1 provides a schematic of a mixed-compression intake, highlighting the interaction bet–ween ramp and cowl shocks and the resulting sepa–ration zone formed by SBLI.

Despite five decades of research[4]many aspects of SBLI remain poorly understood and continue to limit the performance of high-speed vehicles. This has dri–ven ongoing efforts to develop accurate prediction tools and effective flow control strategies.In the con–temporary analysis of supersonic inlet flows, parti–cularly those dominated by Shock-Boundary Layer Interaction (SBLI), high-fidelity methods such as Large Eddy Simulation (LES) have become the standard for investigating transient flow physics. Foundational stu–dies by Loginov et al. [8] and Garnier et al. [9] estab–lished the capability of LES to resolve low-frequency shock unsteadiness and the rich spectral content of turbulent structures, which RANS averages out. More recently, works by Pasquariello et al. [10] and Koo et al. [11]have applied these scale-resolving methods to scramjet geometries, demonstrating their superiority in capturing complex corner flows and mixing pheno–mena. However, the immense computational cost asso–ciated with explicitly resolving the energy-carrying eddies makes LES prohibitively expensive for preli–minary design phases and extensive parametric opti–mization. Consequently, Reynolds-Averaged Navier-Stokes (RANS) models remain the industrial work–horse for comparative investigations. Among these, the k-omega Shear Stress Transport (SST) model has been extensively validated for adverse pressure gradient flows. As highlighted in the comprehensive assessment by Debonis et al. [12], the SST model offers a reliable compromise, accurately predicting the mean separation topology and surface pressure distributionsthe primary metrics of this studyat a fraction of the cost of LES.

To address the adverse effects of SBLI, a wide range of flow control strategies have been developed over the past several decades. These techniques are broadly categorized into passive[13] and active[14] control methods, depending on whether external energy input or moving components are required. Passive methods rely entirely on geometric modifications or surface features to manipulate the flow, Vortex generators (VGs)[15] and micro-vortex generators (MVGs)[16] are among the most widely studied passive devices for SBLI control. By introducing counter-rotating vortices, they entrain high-momentum fluid from the outer freestream into the near-wall region, energizing the boundary layer and delaying separation[17]. Grébert et al.[18] demonstrated through large-eddy simulations at Mach 2.7 that MVGs reduced separation area by ~20% and suppressed low-frequency shock unsteadiness. Similar benefits were reported in hypersonic intakes by Babinsky et al.2009[19], who reported corresponding improvements in intake startability. The primary limitation of VGs, however, lies in their intrusive geometry, which can introduce additional drag and, in some cases, spanwise non-uniformities if not carefully optimized[20]. Zhang et al.[21] demonstrated that placing a two-dimensional bump upstream of the SBLI region can significantly reduce separation when the shock impinges on the bump's convex surface. This improvement is attributed to a combination of precompression from windward compression waves, re-energization of the boundary layer by expansion waves, and vortex weakening via sidewall flow diversion. However, they also observed that control effectiveness is highly sensitive to shock-impingement location, with poor performance when shocks strike the leeward side, highlighting the need for precise placement and alignment of such devices in practical inlets.

Boundary layer bleed[22] has been one of the most practical and extensively used techniques, particularly in mixed-compression supersonic inlets[23]. By remo–ving low-momentum fluid through slots or perforations upstream of the shock impingement, bleeds reduce boundary-layer thickness and delay separation onset [24]. Soltani et al. [25] investigated the influence of boundary-layer bleed location on the stability of a mixed-compression supersonic inlet at Mach numbers 1.8–2.2. Their experimental results showed that the middle bleed slot location (SP12) was the most effective, almost eliminating buzz and significantly suppressing separation over a wide range of operating conditions. While highly effective, bleeds come with penalties in system complexity and mass flow loss, and their performance depends strongly on slot placement and porosity [26]. As a result, they remain a useful but design sensitive tool in SBLI management. Zhai et al.[27] proposed a novel passive control method using a backward facing step (BFS) fixed on the shock generator to mitigate SBLI in a Mach 5 hypersonic inlet. The BFS replaced a strong shock with two weaker ones, which significantly reduced separation bubble length by 62.5%, height by 72.7%, and volume by 90% and improved inlet performance.

While extensive research has explored passive control methods such as micro-ramp vortex generators, surface bumps, bleeds, backward-facing steps[28] there remains a notable gap in the use of chevron shaped grooves for controlling SBLI in supersonic inlets. Most existing methods focus on either vortex induction or flow redistribution through geometric steps, while very rare studies have specifically investigated how sub-boundary layer streamwise vortex generation through chevron grooves can influence the development of separation bubbles and shock stability particularly on the ramp surface upstream of the throat. To address this, the present study introduces and analyses the effect of chevron grooves placed just upstream of the shock foot, aiming to energize the boundary layer and reduce the size of both the primary and secondary separation bubbles. By comparing multiple groove configurations under a fixed Mach 4 condition using CFD analysis, this study provides a novel geometric strategy to improve pressure recovery and flow sta–bility without active mechanisms thereby filling a key gap in current SBLI control research. In this study, three types of chevron grooves were investigated to control shock–boundary layer interaction: shallow (downward) grooves, mid-surface grooves, and upward (protruding) grooves. The shallow grooves, slightly

recessed into the surface, introduce mild near-wall dis–turbances that generate beneficial streamwise vortices. The mid-surface grooves, aligned along the wall surface, offer a balanced interaction creating moderate flow perturbation without significant geometric intru–sion. In contrast, the upward grooves, shaped as small surface protrusions, function like miniature ramps that strongly influence the boundary layer by enhancing mixing and reducing separation more effectively. The following sections detail the computational methodo–logy, validation against experimental data, and a para–metric analysis of these groove configurations.

2. METHODOLOGY

2.1 Geometric details of the model

The geometry adopted in this study is a 2D mixed compression supersonic intake featuring a single-ramp compression surface by Emami and Trexler [29].

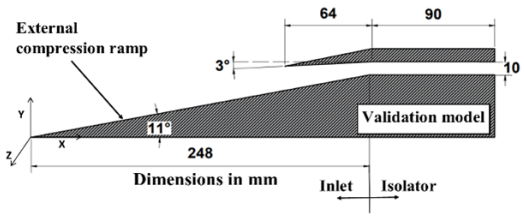

Figure 2. Baseline 2D intake geometry of Emami and Trexler [2] used for numerical validation.

As shown in figure 2, the overall length of the model is 338 mm (L), with the ramp angle set to 11 degrees leading to a throat section. The throat height is 10 mm (H), and the cowl attached to the upper surface is tilted downwards by 3 degrees.

To investigate SBLI control, chevron groove modifications (CGM) were implemented at 215 mm from the leading edge of the ramp, with a span of 20 mm as illustrated in figure 3. This streamwise location was strategically selected as it corresponds to the onset of the primary separation bubble observed in the baseline (uncontrolled) flow field, with the intent of energizing the boundary layer just before it encounters the adverse pressure gradient. Three groove configurations were studied: shallow (case D-1), mid-depth (case M-1), and upward protruding chevrons (case U-1). For this initial comparative study, all three configurations were designed with a consistent groove width (w) of 5 mm, depth (h) of 1.5 mm, and frequency (f) of 4. The term frequency (f) is defined as the number of complete chevron patterns across the 20 mm modification span. The geometric design of these modifications was driven by two primary aerodynamic principles: efficient vortex generation via swept edges and drag minimization through sub-boundary layer placement. First, the chevron topology was selected to maximize streamwise vorticity. Unlike simple transverse grooves, the slanted edges of the chevron induce a spanwise pressure gradient that drives the formation of counter-rotating vortex pairs (CVP). These vortices are critical for entraining high-momentum fluid from the outer boundary layer into the momentumdeficit region near the wall. This mecha–nism is analogous to the mixing enhancement observed in chevron nozzles for jet exhaust noise reduction, where swept trailing edges are used to force rapid shear layer mixing[30]. Second, the specific dimensions were sized according to the principle of sub-boundary layer vortex generation (SBVG)[31]. The groove depth (h=1.5 mm) was explicitly chosen to remain within the incoming boundary layer thickness (δ), which was determined from the baseline simulation to be approximately 4.0 mm at the insertion location (x = 215 mm). By maintaining a ratio of $h/\delta \approx 0.38$, the design aims to energize the logarithmic layer without inducing the excessive wave drag typically associated with protruding vortex generators [32]. Furthermore, the chevron frequency (f = 4) and spanwise width (w = 5 mm) were selected to ensure sufficient spacing bet–ween the generated vortex cores, preventing destructive interference while maintaining a continuous spanwise energization across the separation-prone region.

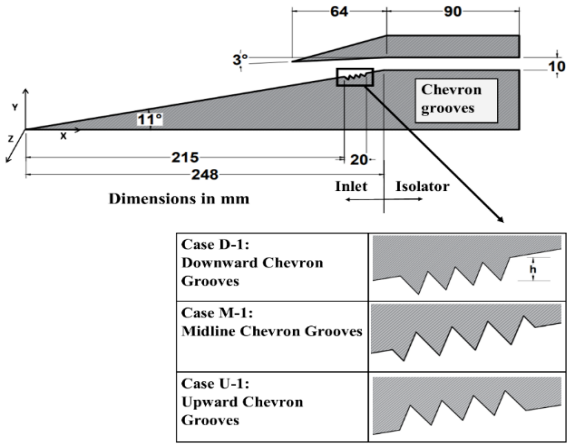

Figure 3. Schematic of the modified intake geometry showing the placement and detail of the Chevron Groove Modifications (CGM).

2.2 Computational setup

Figure 4 shows the computational domain used for the analysis, where the domain height was set equal to the overall length of the baseline intake model. The domain was designed in such a way that the shock generated from the ramp surface could be accurately captured and also minimizing the influence of free-stream boundary effects on the internal aerodynamics.

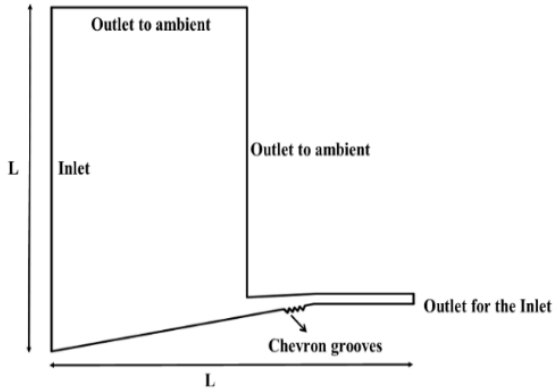

Figure 4. Named selections for the simulation along with computational domain.

Figure 5 depicts the structured grid system for the computational domain, including an enlarged view of the high-resolution mesh in the isolator region. The mesh was generated with high density near the wall and around the chevron features to accurately capture the SBLI phenomena. The final mesh exhibited a minimum Orthogonal Quality of 0.87, a maximum Skewness of 0.12, and a near-wall cell growth rate of 1.2, far exceeding the standard acceptability criteria for finite volume solvers[33] and indicating a very low level of numerical error attributable to cell distortion.

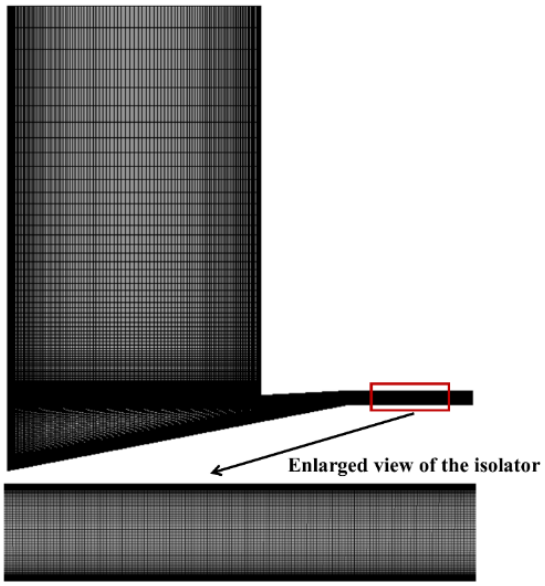

Figure 5. Grid system

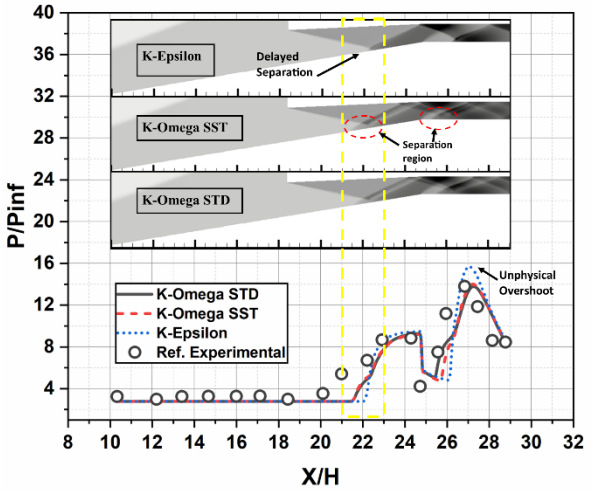

Figure 6. Pressure distribution over ramp surface showing the effect of turbulence models (fine mesh)with pressure contours of respective turbulent model.

The flow solver employs a steady-state, density-based implicit RANS framework, using the k–ω Shear Stress Transport (SST) turbulence model, following the methodology of Coratekin et al. [33][34]. This hybridmodel combines the robustness of the k–ω formulation near walls with the advantages of the k–ε formulation in the free stream, thereby improving predictions in adverse-pressure-gradient and separated flows. As illustrated in Figure 6, the choice of turbulence model significantly alters the predicted shock-boundary layer interaction topology. The pressure contours reveal that the Standard k-epsilon model predicts a visibly smaller and flatter separation bubble at the shock impingement point (X/H ≈22). This under-prediction of the separation extent attributed to the excessive dissipation of the k-epsilon formulation in the near-wall region results in a delayed pressure rise and a significant over-prediction of the peak pressure recovery (P/Pinf ≈16). In contrast, the k-omega SST model captures a larger, physically realistic recircu–lation zone, resulting in a pressure distribution (P/Pinf ≈14) and separation onset location that align closely with the experimental data. Consequently, the SST model, which incorporates a limiter on turbulent shear stress, was selected to ensure accurate resolution of the separation topology. The solver configuration and numerical schemes are summarized in Table 1.

The boundary conditions were defined to accurately simulate the supersonic inlet flow at a freestream Mach number of 4. A pressure-inlet condition was applied to the domain's inlet, where the freestream total pressure (Pt,∞), total temperature (Tt,∞), and the corresponding static pressure (P) is calculated using isentropic rela–tions. The domain exit was modelled as a pressure outlet boundary, with the static pressure set to zero-gauge pressure. All solid surfaces, including the ramp and cowl, were defined with an adiabatic, no-slip wall condition. All simulations were performed at a zero-degree angle of attack. These conditions are summa–rized in Table 2.

Table 1. Solver set-up

Scheme/Parameter	Type/Quantities
Solver precision	Double precision
Solver type	Density based implicit, steady state
RANS	k-ω SST
Spatial discretization	Second-order upwind scheme
Gradient Evaluation	Least squares cell-based
Software	Ansys Fluent 2019

Table 2. Boundary conditions

Boundary Type	Condition Applied
Inlet [Pressure inlet]	Total pressure $P_{t,\,inf}$ = 308145 Pa Static pressure P = 2029.468 Pa Total temperature $T_{t,\,inf}$ = 300 K
Outlet/Outlet to ambient [Pressure outlet]	Static pressure P (zero)
Ramp, Cowl [Wall]	No-slip, adiabatic

2.3 Validation and Grid Independence Test

To ensure the numerical solution is independent of spatial discretization errors, a comprehensive grid sensitivity study was conducted. Three distinct mesh resolutions Coarse, Fine (Baseline), and Super Fine were evaluated. These grids differed in both global cell count (to check free-stream convergence) and first-layerheight (to verify near-wall y^+ resolution for the turbulence model). The detailed parameters for each grid level are summarized in Table 3.

As shown in Figure 7, the grid effects are visualized using annotated pressure contours and pressure distri–

butions. To aid interpretation, yellow vertical lines highlight the difference in shock location in the contours. Additionally, red circles on the contours highlight the specific region where the Coarse mesh blurs the reflected shock, causing the smearing observed in the pressure data.Consequently, the Coarse mesh failed to capture the sharp pressure inflection at the shock impingement point (X/H ≈ 27) due to numerical smearing in the buffer layer. In contrast, the Fine and Super-Fine meshes produced nearly identical pressure distributions, confirming grid convergence at $y^+ \approx 1$. This indicates that the fine mesh offered an optimal balance between accuracy and computational cost, and it was therefore selected for all further simulations.

Table 3. Grid independence and near-wall resolution parameters

Mesh Type	Mesh Count	First Layer Height $(\Delta \dot{y}) \times 10^{-5}$	y^+_{avg}	y^+_{max}
Coarse	20,000	9.86	11.64	18.24
Fine	80,000	0.64	0.77	1.38
Superfine	1,20,000	0.18	0.18	0.33

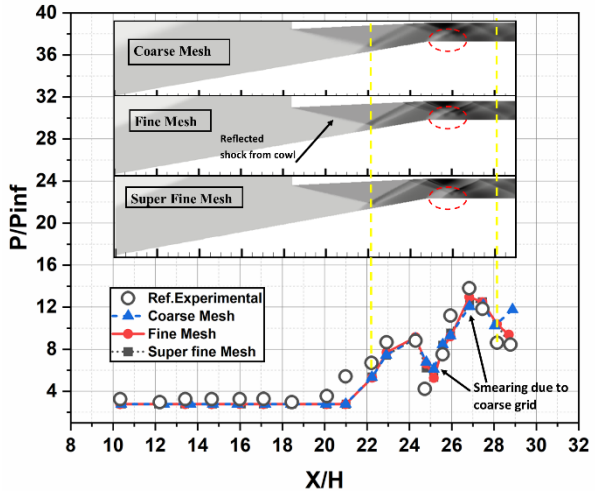

Figure 7. Grid independence check

The fidelity of the current numerical model was established by comparing the simulated pressure distribution along the lower ramp against both experimental measurements from Emami and Trexler [29] and three-dimensional computational findings from Saha and Chakraborty [35]. This comparison is presented graphically in Figure 8, where wall pressure is non-dimensionalized by the freestream static pressure (P∞) and the streamwise coordinate is normalized by the intake's throat height (H).

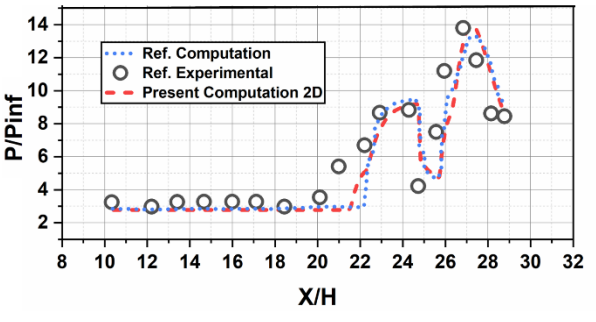

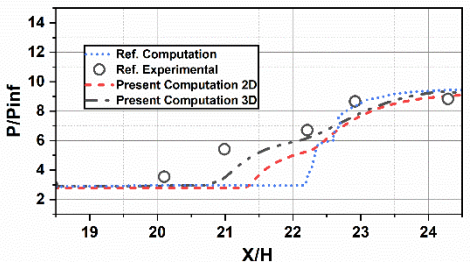

Figure 8. Comparison of present numerical results with reference data. Top: 2D computations against experimental [29] and computational [35] results. Bottom: 3D and 2D computations over the specified region for detailed validation.

To capture baseline physics more effectively, a full 3D simulation of was performed. As highlighted in the inset of Figure 8, the 2D simulation predicts a delayed separation onset compared to the experiment, a known limitation of 2D RANS which artificially constrains the separation bubble. However, the 3D simulation captures the upstream influence of the separation much more accurately, initiating the pressure rise at X/H ≈20.8, which aligns closely with the experimental data. This confirms that the primary deviation is due to 3D relief effects, and the 2D model remains a valid, conservative tool for the comparative parametric study.

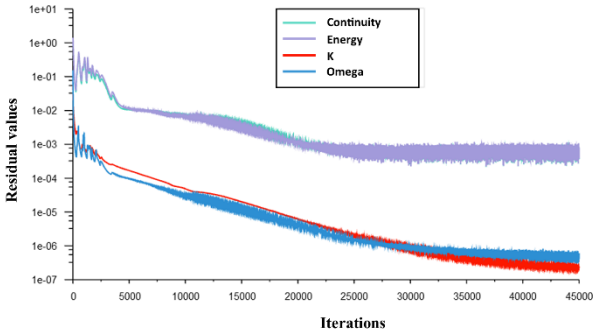

Figure 9. Residual plot, showing the convergence criteria.

Convergence was monitored using residual histories and mass flow balance. As shown in Figure 9, residuals for continuity and energy stabilized below 10^{-3} while turbulence quantities dropped below 10^{-6}. The net mass flow imbalance was maintained below 0.1%, ensuring a physically converged solution.

3. RESULTS AND DISCUSSION

3.1 Base Case Flow Behaviour Analysis

To understand the baseline flow characteristics of the supersonic intake, a simulation was carried out at a freestream Mach number of 4. Figure 10 illustrates the Mach number contour within the intake. The external compression shock generated from the ramp reflects off the cowl lip, forming a system of oblique shocks that propagate downstream. This interaction is visible in the isolator region, indicating successive shock reflections typical of mixed-compression inlets.

However, the shock reflections also result in an adverse pressure gradient near the lower wall. As the boundary layer, which is already weakened by viscous effects, interacts with this gradient, it separates from

the surface. This forms a visible separation layer extending downstream. To further investigate the separation behaviour, Figures 11[a] and [b] show the velocity vector field and velocity streamlines within the inlet. The velocity vectors clearly highlight a large recirculation zone near the ramp and isolator junction. This reversed flow region arises due to the breakdown of boundary layer integrity under strong compression, causing low-momentum flow to separate. Such flow separation can trigger total pressure loss, non-uniform flow at the engine face, and even engine unstart under off-design conditions [36]. The flow reversal behaviour agrees with the SBLI physics described by Settles [37] and observed in high-speed intake testing by Vuković D et al. [38].

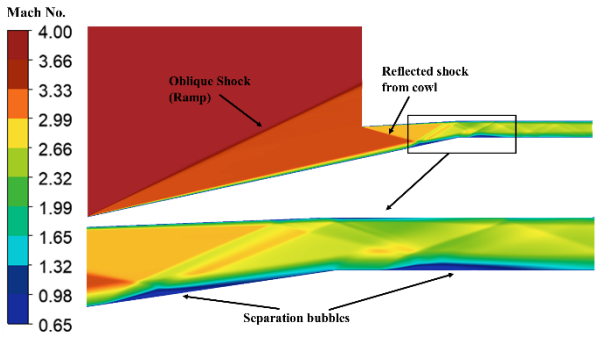

Figure 10. Mach contour of base case at Mach 4

To quantify the aerodynamic penalties due to flow separation, key performance and flow quality metrics were extracted from the simulation data. These include the Total Pressure Recovery (TPR), Distortion Coefficient (DC), and a dimensionless Separation Factor (SF) measured at two critical regions around the separation bubble on the ramp [atX/H=0.656] and at the throat [at X/H=0.781].These parameters have been widely recognized in literature as crucial indicators of intake performance. According to study of Askari et al.[39] and Sepahi-Younsi et al.[40], the main objective of an air intake system is to ensure both quantitative and qualitative delivery of airflow to the engine's combustion chamber.

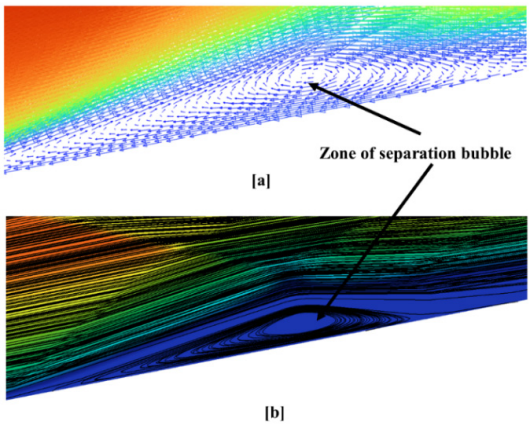

Figure 11. Velocity vector[a] and Velocity streamline [b] contour inside the intake showing separation zone.

Achieving this requires maximizing the recovery of total pressure while minimizing flow distortion at the intake exit. TPR assesses the ability of the intake to preserve total pressure from the freestream to the engine face, which is critical for maintaining thrust and combustionstability.

$$TPR = \frac{\left(P_{t,exit}\right)avg}{P_{t,\infty}} \tag{1}$$

where $(P_{t,\ exit})_{avg}$ and $P_{t,\ inf}$ are total pressures at the exit (average) and inlet planes, respectively.

The Distortion Coefficient (DC) indicates the uniformity of flow at the intake exit; a lower distortion index reflects more even flow conditions, reducing the risk of engine surge or stall. The DC is defined as the absolute value of the differences between the maximum total pressure and the mean value of the total pressure at the rake station normalized by the mean total pressure.

$$DC = \frac{P_{t_{max}} - P_{t_{avg}}}{P_{t_{avg}}} \tag{2}$$

where $P_{t_{max}}$ and $P_{t_{avg}}$ are maximum and average total pressure respectively.

Finally, The Separation Factor (SF) provides a compact measure of bubble extent by incorporating both its length and height. It is defined as

$$SF = \frac{L_{sep} + H_{sep}}{2H} \tag{3}$$

where L_{sep} and H_{sep} are the bubble length and height, and H is the throat height. A lower SF corresponds to a smaller separation region, thereby indicating improved boundary layer control.

In table 4. Summarizes these critical performance parameters have been evaluated for the baseline case to understand the behaviour of the supersonic intake flow. The bubble dimensions specifically measured at ramp bubble length (L_{sep}) 21.85 mm and height (H_{sep}) 1.189 mm, throat bubble at 21.53 mm (L_{sep}) and 1.186 mm (H_{sep}). The average Total Pressure Recovery (TPR) was calculated at the midpoints of both separation bubbles to quantify how much of the total pressure is retained after the shockboundary layer interactions. Additionally, the Distortion Coefficient is critical for stable combustion. Together, these parameters provide a comprehensive picture of the aerodynamic performance and are used as benchmarks for comparing subsequent geometrical modifications.

Table 4. Performance Parameters for Base Case

Parameter	At X/H=0.656 [Ramp Bubble]	At X/H=0.781 [Throat Bubble]
Avg. Total Pressure Recovery	0.6498	0.5493
Distortion Coefficient (DC) (%)	31.81	53.58
Bubble Height (H_{sep}) (mm)	1.189	1.186
Bubble Length (L_{sep}) (mm)	21.85	21.53
Separation Factor (SF)	1.15	1.13

3.2 Performance Assessment of Modified Chevron Cases (Part 1)

In this section, the performance of three geometrical modifications Case D-1, Case M-1, and Case U-1 is evaluated to investigate the influence of different chevron groove placements on shock–boundary layer interaction (SBLI) and overall intake performance. Across Case D-1 to Case U-1, significant differences in flow behaviour are evident when examining the Mach number contours (figure 13). The introduction of chevron grooves modification alters the near-wall flow field significantly by manipulating the SBLI. By introducing chevron grooves on the ramp in Case D-1, a periodic surface disturbance is created just upstream of the expected separation zone. These shallow down–ward grooves act as passive flow control elements by introducing streamwise vortices into the boundary layer. These vortices enhance near-wall momentum exchange, thereby energizing the boundary layer and resisting adverse pressure gradients caused by the im–pinging shock. To quantify these effects, a Separation Factor (SF) was defined from bubble contours by applying a cutoff of 150 m/s in x-velocity to isolate the separated region (figure 14). The effect is modest on the ramp, where the Separation Factor (SF) increases slightly from 1.15 (Base case) to 1.44, but the throat separation reduces sharply, with SF at throat dropping from 1.13 to 0.55. Case M-1 features a mid-groove configuration, where the grooves are neither fully downward nor fully upward but moderately indented into the wall. Com–pared to Case D-1, the throat separation is further suppressed, with SF at throat dropping to 0.21, but this comes at the expense of a continued rise in ramp separation, where SF at ramp increases to 1.57. In Case U-1, where the chevron geometry is elevated upward (raised chevrons), the interaction becomes more aggressive. These upward grooves act like miniature compression ramps, generating stronger local shocks and more energetic vortical structures. The intensified vortex strength leads to improved momen–tum transfer but also introduces localized disturbances. As a result, the ramp separation grows slightly (SF at ramp = 1.52), but the throat bubble almost vanishes, with SF at throat collapsing to 0.19.This reduction of ~83.1% confirms that limiting the device height to within the boundary layer ($h<\delta$) does not compromise control authority; rather, it effectively suppresses separation without the need for large, drag-inducing protrusions. To further clarify the mechanism behind these SF trends, velocity vector plots are examined for the Base case and Case U-1(figure 15) These reveal the formation of strong counter-rotating vortices above the chevron grooves, which energize the boundary layer and explain both the collapse of throat separation and the redistribution of ramp recirculation observed in the contour analysis. These trends are consistent with findings by Panaras et al. [20], who documented that stronger streamwise vortices can suppress SBLI-induced separation, particu–larly at critical regions like the isolator entrance or intake throat. Additionally, works like Grebert et al. [41] show that VGs and micro-ramp structures influence bubble size and shock foot oscillation depending on placement and geometry.

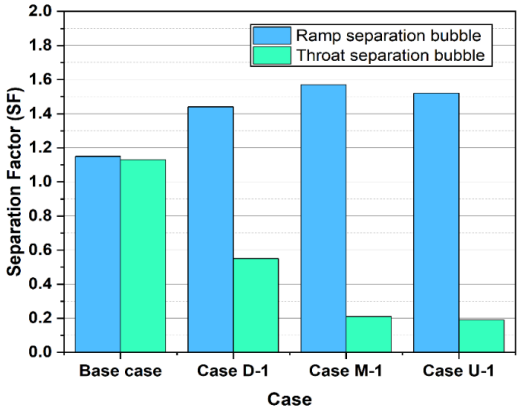

Figure 12. Bar graph showing Separation Factor (SF) comparison between base case and modified cases at ramp and throat. Figure 12. Bar graph showing Separation Factor (SF) comparison between base case and modified cases at ramp and throat.

The Total Pressure Recovery (TPR) was assessed at six different lines across the intake geometry to identify local improvements in flow quality due to the chevron groove modifications. (figure 16) At Line-1, located at the mid of ramp separation bubble [X/L=0.656], did not show significant improvements in the modified cases compared to the Base case. This indicates that, although the chevrons energize the boundary layer locally, their influence is insufficient to fully suppress the initial separation. At Line-3, situated near the throat entrance, the TPR distribution in Cases M-1 and U-1 closely follows the baseline, while Case D-1 performs worse due to weaker vortex energization.

The most notable improvement is observed at Line-4, positioned at the mid-point of the throat separation bubble [at X/L=0.781]. Here, all modified cases de–monstrate a marked rise in TPR compared to the baseline, with Case U-1 and M-1 delivering the stron–gest gains. This enhancement directly correlates with the significant reduction in throat SF, which quantifies the collapse of the baseline bubble. Downstream, at Line-6 (intake exit), Case U-1 achieves the highest TPR, followed by M-1, while D-1 continues to trail.

The surface pressure distribution along the ramp, presented in Figure 17, highlights the influence of chevron groove modifications on shock structure and near-wall gradients. In the Base case configuration, the P/Pinf trace is characterized by successive sharp rises followed by oscillations, directly associated with multiple shock reflections generated by the large throat bubble. These oscillations in zones 3–6 reveal strong SBLI and repeated shock impingement, consistent with severe flow unsteadiness. In contrast, the modified cases show distinct alterations across the six high–lighted zones. In Zone 1 (X/H≈21.5–23.5), coinciding with the chevron placement, Cases M-1 and U-1 ex–hibit a noticeable dip in pressure compared to the base case, reflecting localized disturbance from vortex generation, whereas Case D-1 closely follows the baseline behaviour in zone 1 and 2, indicating weaker influence. The most pronounced difference arises in Zone 3 (X/H≈25–27), where the baseline shows a sharp single rise in P/Pinf, corresponding to the throat shock interaction. In contrast, the modified cases display three smaller peaks, repre–senting fragmented and redistributed shocks.

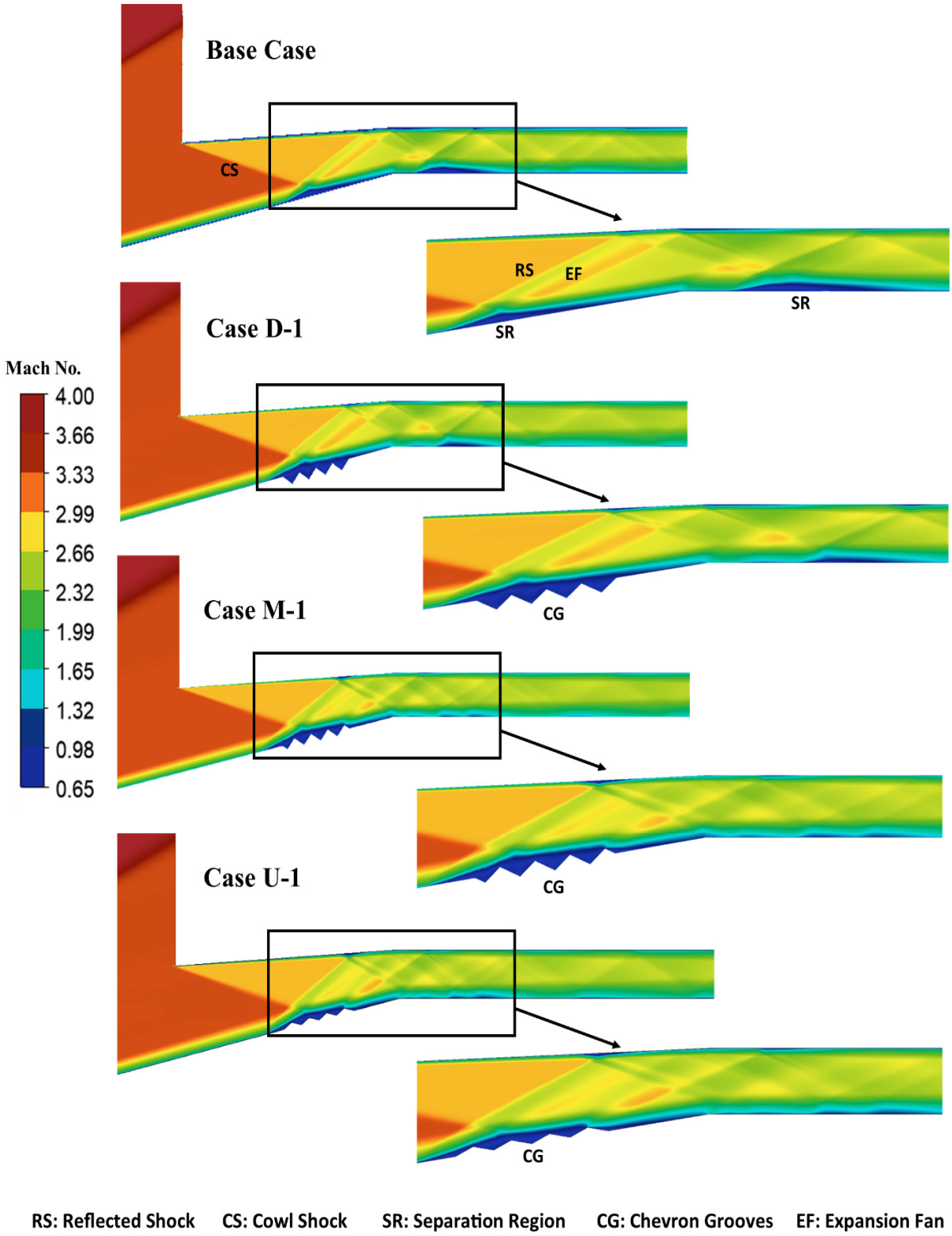

Figure 13. Mach contours of 3 modified cases compared with base case at Mach 4.

This splitting of the shock front into weaker components is a direct manifestation of vortex-induced re-energization of the boundary layer, which prevents the accumulation of a single strong separation-driven reflection. Similar behaviour has been reported in repeated backward-facing step (RBFS) configurations by Vijay et al.[28], where strengthening of reattachment promotes the merging of reflected and compression shocks into a single weaker wave at lower height, thereby reducing SBLI intensity. Downstream, in Zones 4–6, the baseline trace shows consecutive oscillations, with alternating rises and falls in pressure, indicating strong reflected-shock/bubble coupling. By comparison, the modified cases replace these oscillations with a smoother trend. Case U-1 and M-1 demonstrate a significant dip at X/H≈29, followed by a single

attenuated peak, showing that multiple strong reflections have been replaced by a single weakened structure. This behaviour is consistent with the observed reduction in throat separation (low SF values) and smoother TPR recovery at the exit. Overall, the contour and line-plot evidence corroborate the shock-weakening mechanism: rather than eliminating shocks, chevron-induced vortices redistribute them into multiple weaker events upstream (Zones 1–3), while suppressing repeated downstream reflections (Zones 4–6). This transition reduces overall oscillatory loading, stabilizes the pressure field, and supports the observed improvements in both Total pressure recovery (TPR) and Separation factor (SF).

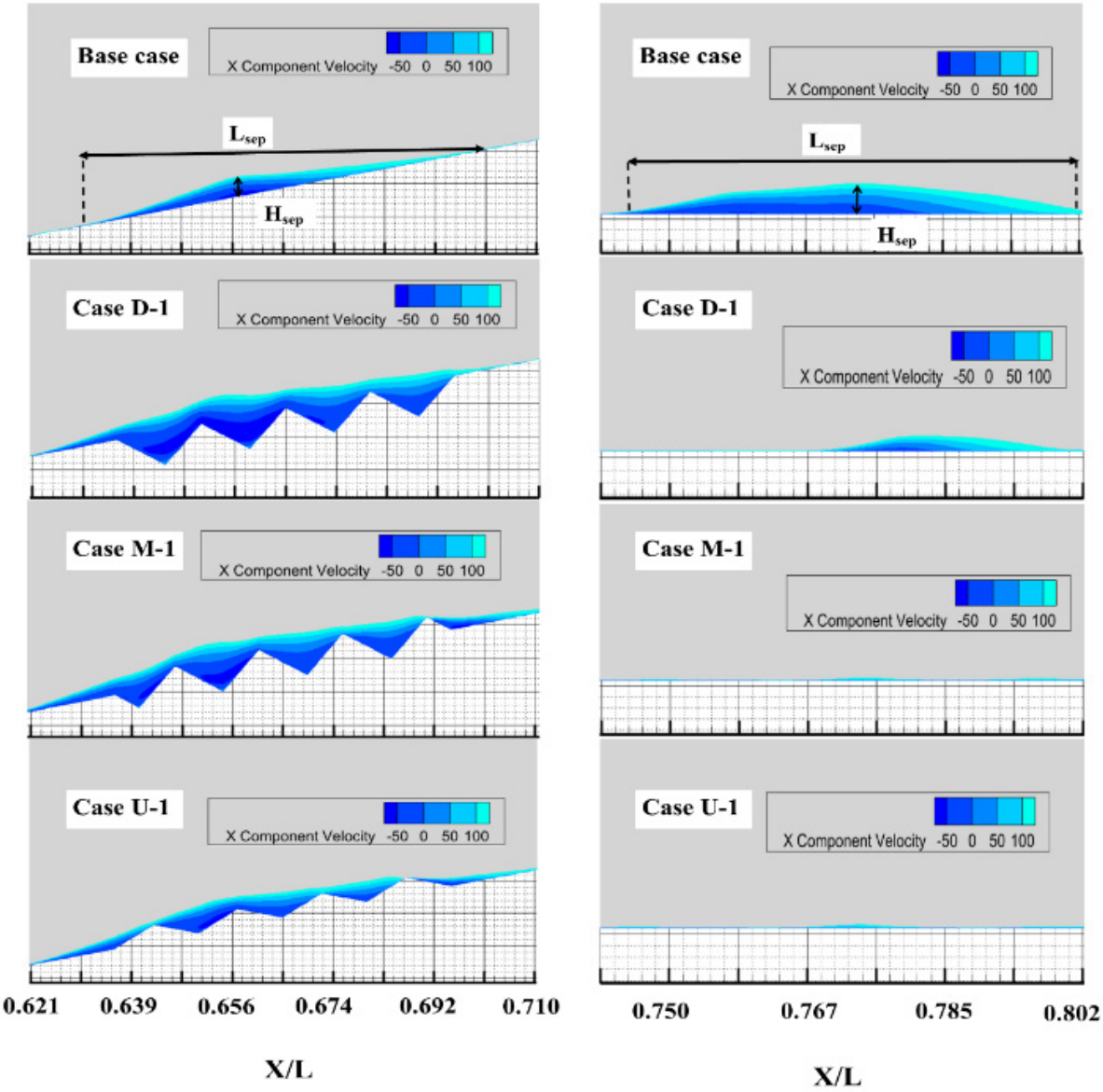

Figure 14: Bubble size comparison [x-velocity contour cut off at 150m/s] of base case with 3 modified cases at ramp and throat separation region.

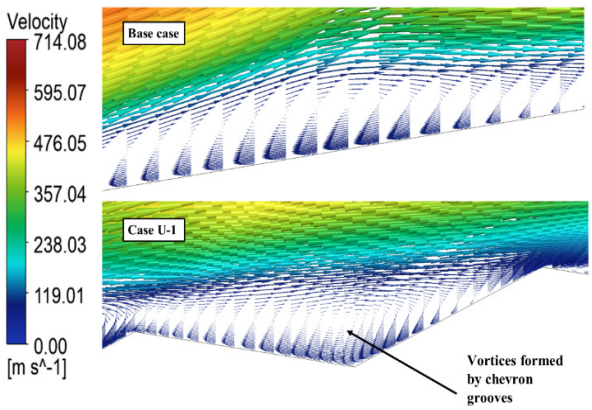

Figure 15. Velocity vector plot of Base and Case U-1 showing vortex formed by chevron grooves.

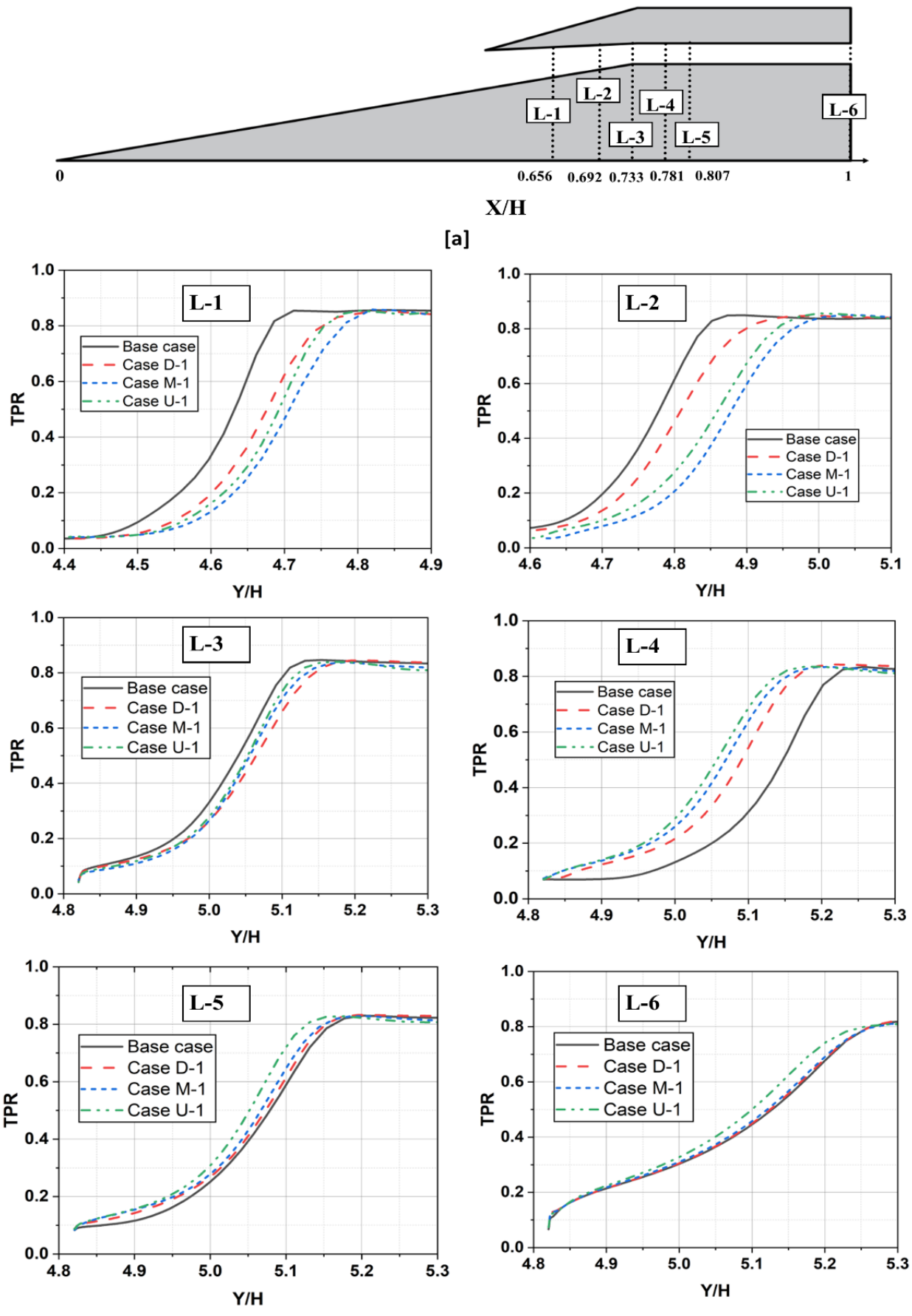

Figure 16. [a] Baseline intake geometry showing six probe lines (L-1 to L-6) used for flow evaluation. [b] Variation of Total Pressure Recovery (TPR) along the six lines for the base case and modified cases, illustrating the effect of chevron groove modifications on local pressure recovery.

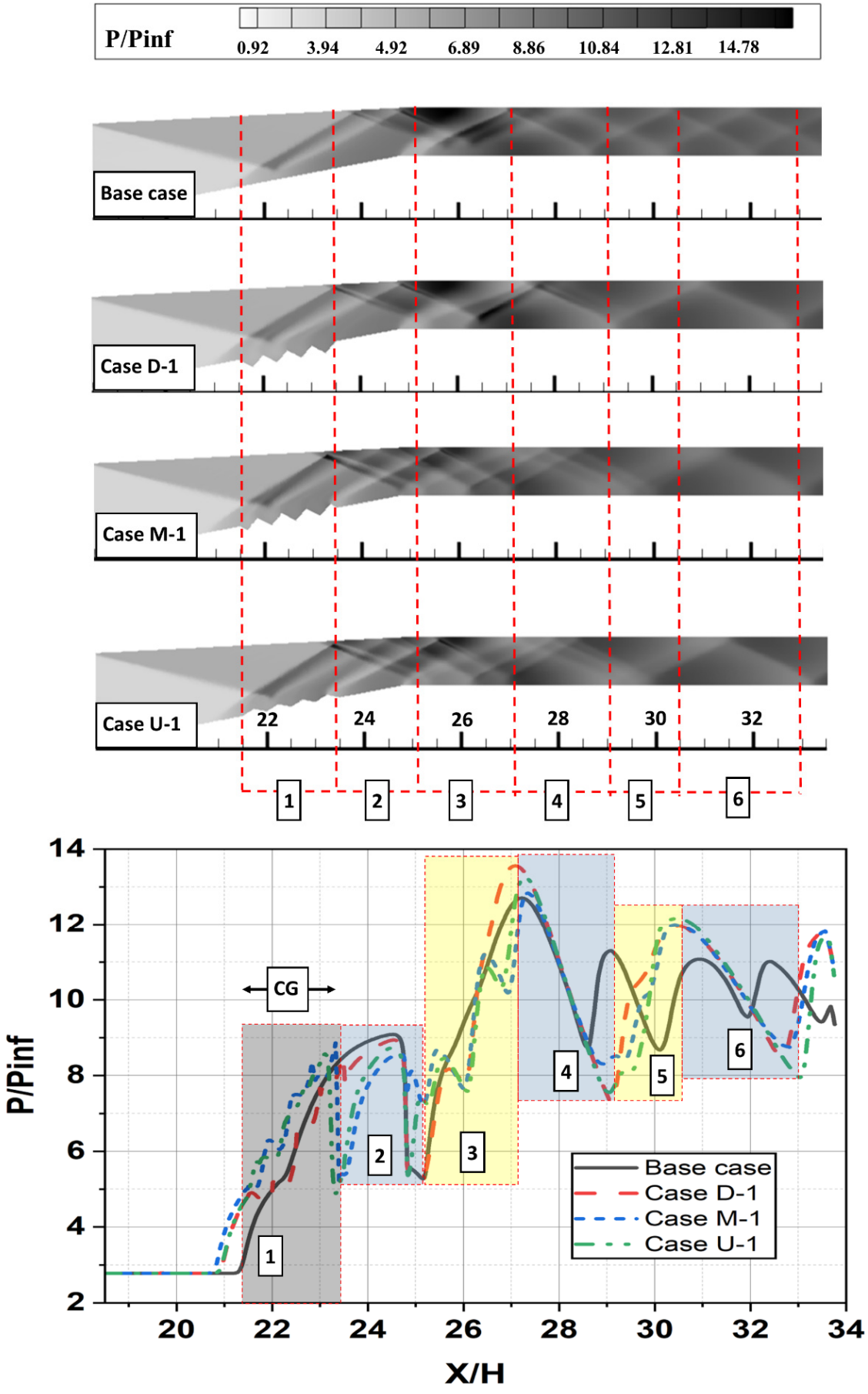

Figure 17. Surface pressure distribution on the ramp (P/Pinf) for the base case and modified cases, presented as both contour plots and line graphs. The results illustrate differences in shock structures and near-wall pressure gradients induced by chevron groove modifications.

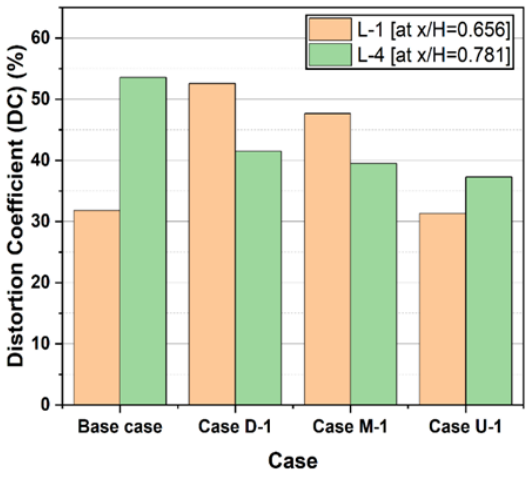

Figure 18. Distortion Coefficient (DC) comparison at Line-1 x/H = 0.656 (ramp) and Line-4 X/H = 0.781 (throat) for the base case and modified chevron groove cases. Values are extracted at the location of maximum height of the respective separation bubbles.

The Base Case showsDistortion Coefficient (DC) values of 31.81% at Line-1 (ramp, X/H = 0.656) and 53.58% at Line-2 (throat, X/H = 0.781), both located at the midpoints of their respective separation bubbles. In Case D-1, ramp distortion rises sharply by ~65% to 52.59%, while throat distortion decreases by ~23% to 41.47%, reflecting an unfavourable trade-off. Case M-1 lowers throat distortion further to 39.49% (~26% lower than baseline) but still increases ramp distortion by ~50% to 47.65%.

The most favourable outcome is achieved in Case U-1, where ramp distortion remains nearly unchanged (31.35%, ~1% lower) and throat dis–tortion drops significantly to 37.30% (~30% lower). These results highlight U-1 as the most balanced configuration for minimizing overall distortion.

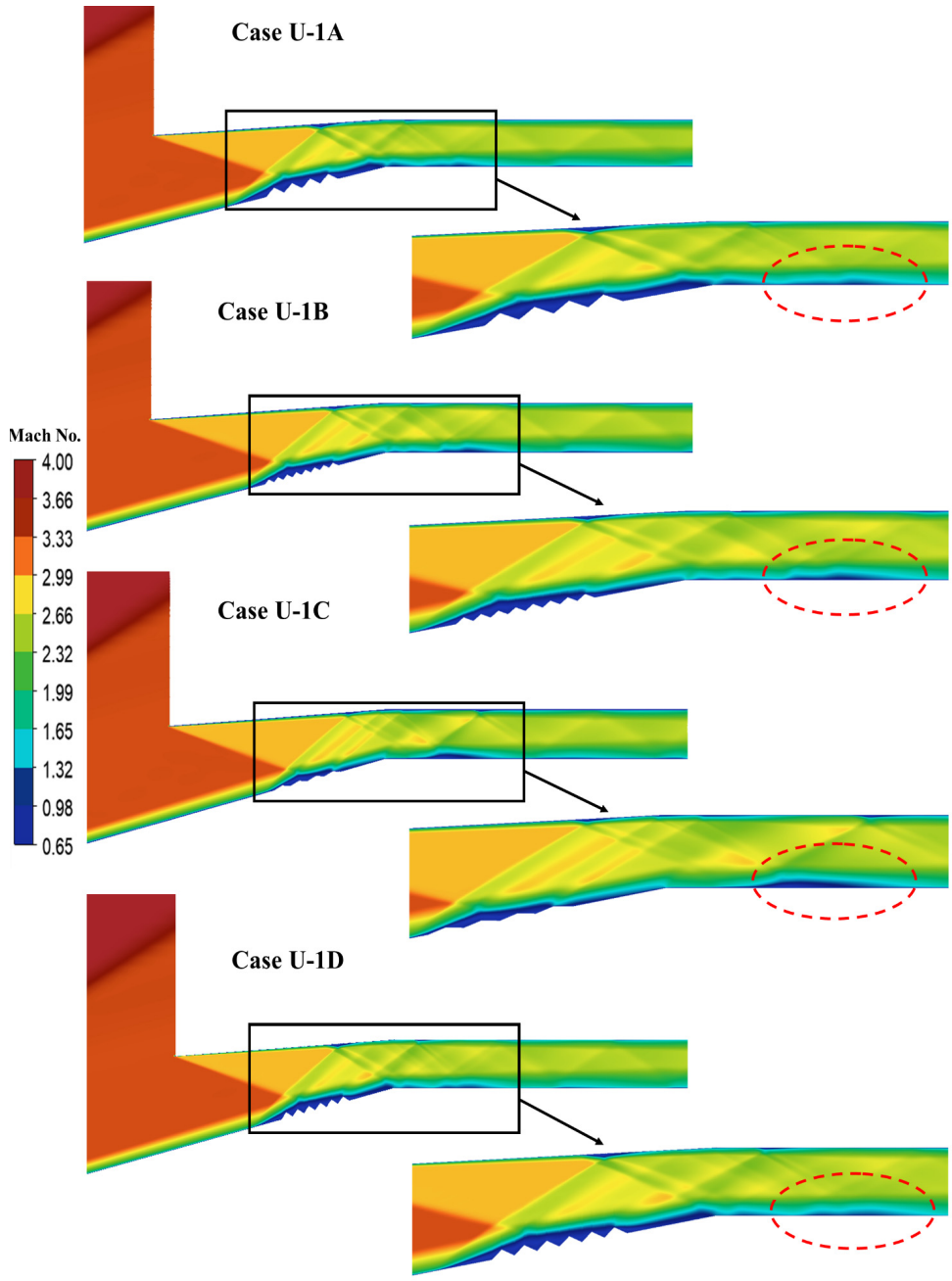

Figure 19. Mach contours of 4 modified cases of case U-1 at Mach 4

3.3 Parametric Evaluation of Upward Chevron Groove Modifications (Part 2)

Building upon the promising results of the upward chevron configuration (Case U-1), a second phase of investigation was carried out to assess the sensitivity of the performance to groove depth and frequency. In this section, four variants of Case U-1 were explored each designed to test different groove characteristics while keeping other geometric and boundary parameters constant.The objective of the study was to analyse how small changes in surface geometry can influence flow separation behaviour, shock boundary layer interaction (SBLI), and ultimately, the intake's aerodynamic performance. Figure 18. Mach number contours for the parametric variants (U-1A to U-1D).

Table 5. Geometrical variants of Case U-1

Cases	Depth of chevron grooves(*h*)(mm)	Frequency of chevron(*f*)
Case U-1A	2	4
Case U-1B	1	8
Case U-1C	1	4
Case U-1D	1.5	6

The Mach contours highlight differences in separation regions and shock structures caused by variations in groove height and frequency.

In Case U-1A (h = 2 mm, f = 4), the deeper grooves generate stronger upstream disturbances, leading to an increased ramp separation extent (SF at ramp = 1.98). Although throat separation decreases relative to the Base Case (SF at throat = 0.149), the larger ramp bubble suggests excessive vortex penetration and non-uniform reattachment. This result explicitly confirms that inc–reasing the device height beyond the boundary layer thickness is detrimental to performance. Case U-1B (h = 1 mm, f = 8) demonstrates the most favourable behaviour, achieving balanced suppression of both ramp and throat separation (SF at ramp = 1.56, SF at throat = 0.21). The high-frequency shallow grooves promote efficient vortex mixing, which energizes the boundary layer and facilitates earlier reattachment, yielding the cleanest streamline alignment among all tested variants of Case U-1. Case U-1C (h = 1 mm, f = 4) performs poorly compared to other configurations, with weak vortex generation resulting in reduced near-wall energization. This leads to lower ramp control (SF at ramp = 1.20) but the largest throat separation among all U-1 variants (SF at throat = 0.62). The Mach contours further reveal diffuse shock structures and persistent reversed flow, indicatingincomplete recovery of the boundary layer. Case U-1D (h = 1.5 mm, f = 6) yields intermediate results, with moderate improve–ments over the base case (SF at ramp = 1.81, SF at throat = 0.19). While the separation extent in U-1D is reduced compared to U-1A and U-1C, it remains less effective than the optimal U-1B case.

The Total Pressure Recovery (TPR) distributions at Line-4(X/H =0.781), shown in Figure 21, highlight the comparative behaviour of the Case U-1 variants. The original Case U-1 maintains the best recovery profile, with the highest average TPR and a smooth rise across the separation zone. Variants Case U-1B and U-1D follow closely, nearly overlapping the Case U-1 curve, suggesting that while they retain effective separation control, they do not deliver any significant improvement beyond the baseline U-1. By contrast, Case U-1A exhibits slightly reduced recovery, and Case U-1C shows the weakest performance, with lower TPR values and more pronounced deviation from the optimal profile.

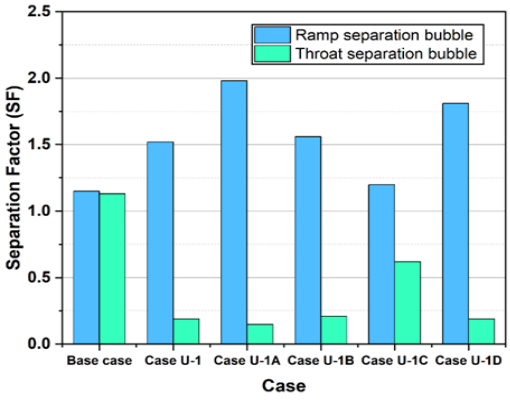

Figure 20. Bar graph showing Separation Factor (SF) comparison between Base case, Case U-1 and Case U-1A to U-1D at ramp and throat.

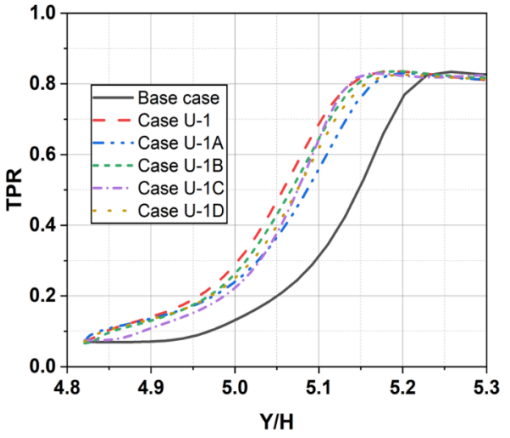

Figure 21.Variation of Total Pressure Recovery (TPR) between Base case, Case U-1 and Case U-1A to U-1D at L-4(X/H = 0.781).

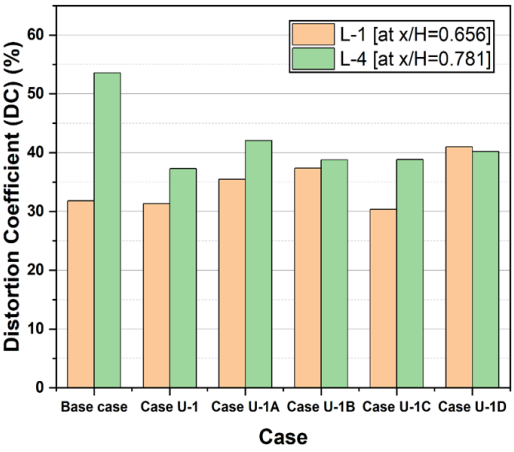

Figure 22. Distortion Coefficient (DC) comparison at Line-1 X/H = 0.656 (ramp) and Line-4 X/H = 0.781 (throat) for the Base case, Case U-1 and Case U-1A to U-1D. Values are extracted at the location of maximum height of the respective separation bubbles.

The base case exhibits the highest distortion (53.58%), highlighting severe non-uniformity at the throat. In contrast, Case U-1 and all variants of Case U-1 achieve lower DC, confirming their effectiveness in stabilizing the intake flow. Like Case U-1, Case U-1B show the most favourable performance, with DC values of 38.8%, indicating smoother pressure distri–bution and reduced risk of unstart. Case U-1C also registers a comparable DC of 38.83%, but its asso–ciated flow features suggest weaker suppression of the throat bubble. U-1D (40.19%) and U-1A (42.08%) perform moderately, still improving over the baseline but less effective than Case U-1/U-1B.

Overall, the bar graph clearly demonstrates that up–ward chevron grooves particularly at optimized depth and frequency can substantially reduce distortion levels, with Case U-1B emerging as the most balanced configuration.

3.4 Performance Sensitivity to Freestream Mach Number Variation

The operational robustness of the control device was evaluated by varying the freestream Mach number (M_∞ = 4.0 to 2.5) .This imposes a severe aerodynamic challenge, as lower Mach numbers result in steeper shock angles and increased potential for intake unstart. At the intermediate off-design conditions of Mach 3.5 and 3.0, both the Base–line and Controlled configurations remain started. As shown in Figure 23 [a] and [b] the shock structures are stable. Quantitative analysis at the throat (Line-4) reveals a slight performance crossover in these regimes. At Mach 3.5, the Base Case achieves a TPR of 0.644 (DC = 36.92%), while Case U-1 yields a slightly lower TPR of 0.634 (DC = 38.57%). Similarly, at Mach 3.0, the Base Case outper–forms the controlled case with a TPR of 0.744 versus 0.682. This suggests that at these specific intermediate Mach numbers, the baseline shock-boundary layer interaction is naturally less severe due to the favou–rable Reynolds number and shock angles; consequently, the mixing losses introduced by the chevrons slightly outweigh their separation control benefits.

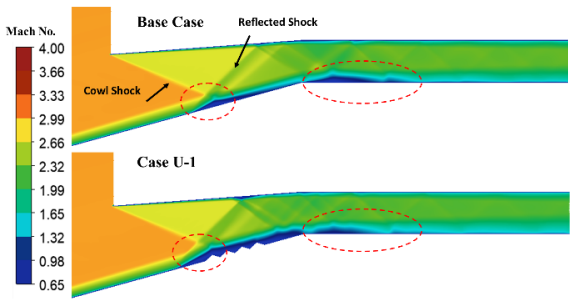

[a]

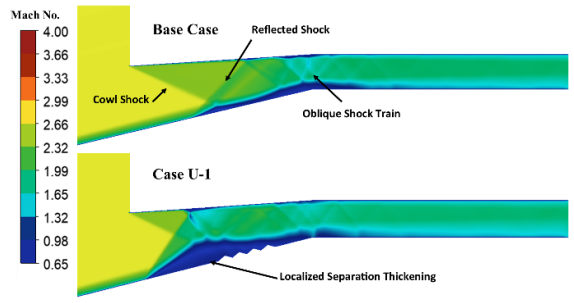

[b]

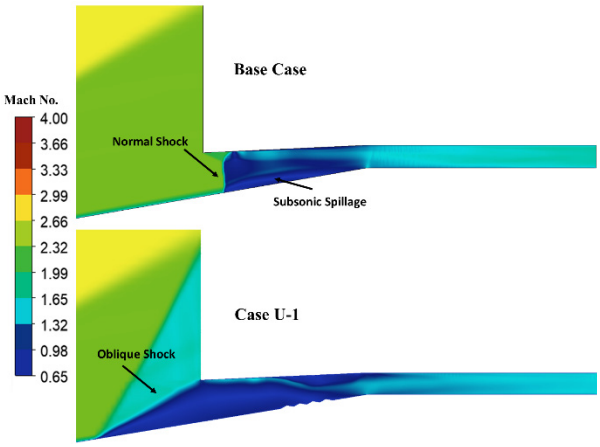

[c]

Figure 23: Comparison of Mach contour of base case with case U-1 at different free stream Mach numbers [a] Mach number 3.5 [b] Machnumber 3.0and [c] Mach number 2.5

However, the critical value of the chevron design is revealed at the operational limit, Mach 2.5. As illus–trated in Figure 23 [c] , the Base Case suffers a catas–trophic unstart, characterized by a detached normal shock standing upstream of the cowl and subsonic spil–lage at the inlet face. In stark contrast, Case U-1 suc–cessfully maintains a soft start, supersonic flow regime with an attached oblique shock system. While the baseline fails completely, the chevron configuration prevents the throat from choking, effectively extending the intake's stable operating range by 0.5 Mach number. This confirms that the sub-boundary layer chevrons provide a critical stability margin that prevents air intake unstart during severe off-design excursions.

3.5 Three-Dimensional Validation

To rigorously validate the findings of the 2D parametric study, full three-dimensional (3D) RANS simulations were performed for both the Baseline and the optimized Case U-1. This analysis ensures that complex three-dimensional flow phenomena do not negate the performance benefits observed in the 2D approximations. The flow topology on the symmetry plane is compared in Figure 24. The 3D simulations exhibit a shock structure and separation topology that is remarkably consistent with the 2D predictions. In the Baseline configuration, both 2D and 3D results show a large, low-momentum separation region at the throat. In Case U-1, the 3D simulation confirms that the chevron-generated vortices effectively suppress this recirculation zone, maintaining a thinner and more attached boundary layer through the interaction zone just as predicted in 2D.

The underlying control mechanism is further visua–lized in Figure 25 using iso-surfaces of Q-criterion. This confirms the formation of stable Counter-Rotating Vortex Pairs (CVP) in the full 3D flow field, which are responsible for the entrainment of high-momentum fluid observed in the Mach contours.

Finally, the flow quality improvement is quantified in Figure 26, which compares the Total Pressure Reco–very (TPR) profiles at the throat (Line-4). The results reveal critical insights regarding the flow physics. The

2D Baseline and 3D Baseline profiles show excellent agreement in the near-wall region (Y/H < 5.2), con–firming that the 2D solver accurately captures the fundamental SBLI physics of the uncontrolled intake. Most importantly, the 3D Case U-1 demonstrates a substantial improvement in pressure recovery compared to the 3D Baseline. Although the 2D model predicts a slightly higher recovery than the 3D model, the trend is identical. The 3D configuration retains most of the predicted gain, confirming that the 2D parametric study was a valid, computationally efficient, and slightly conservative tool for optimizing the chevron geometry.

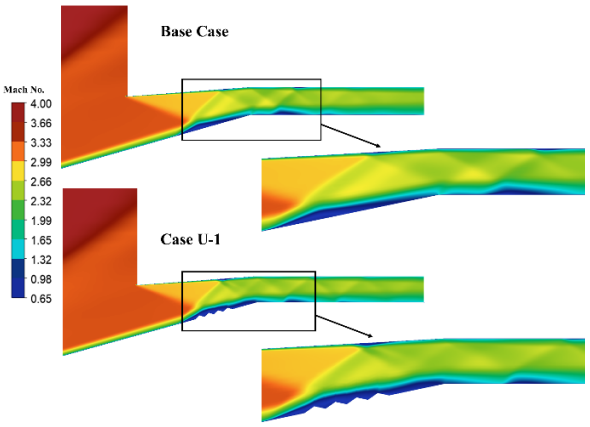

Figure 24. Comparison of Mach number contours of base case and case U-1 on the symmetry plane.(3D)

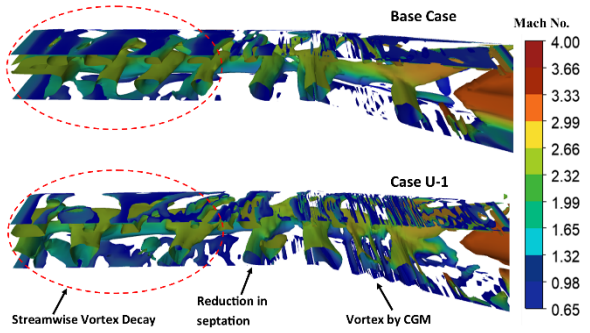

Figure 25. Iso-surface of Q-criterion coloured by Mach number of base case and case U-1.

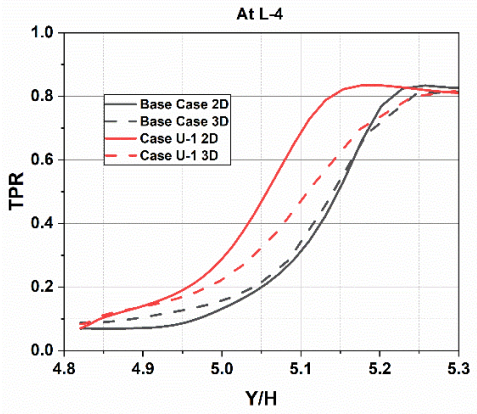

Figure 26. Comparison of Total Pressure Recovery (TPR) profiles at the throat (Line-4). (2D vs 3D)

4. CONCLUSIONS AND FUTURE SCOPE

This study evaluated the effectiveness of Chevron Groove Modifications (CGM) as a passive flow-control strategy for mitigating shock–boundary layer interaction (SBLI) in a Mach 4 mixed-compression intake. The baseline configuration exhibited large recirculation zones, particularly at the ramp and throat bubbles, leading to significant pressure losses and distortion, with throat bubble lengths extending up to 21.53 mm and DC reaching 53.58%.Three primary groove placements were tested. Among them, the upward chevron configuration (Case U-1) demons–trated the strongest control authority, collapsing the throat bubble by ~83%, reducing distortion to 37.3%, redistributing multiple strong shock reflections into weaker, more stable structures, and significantly smoo–thing the pressure recovery profile. To generalize the control physics, four variants of U-1 were examined. Results showed that effective SBLI suppression requires (i) maintaining groove height below the local boundary-layer thickness (h < δ) and (ii) using high-frequency, shallow grooves to promote stable counter-rotating vortex pairs without inducing excess wave drag. Based on these criteria, Case U-1B (h = 1 mm, f = 8) emerged as the optimal design.

A comprehensive off-design Mach-number study revealed that while both baseline and CGM configu–rations remain started at Mach 3.5–3.0, the baseline intake undergoes complete unstart at Mach 2.5 due to a detached normal shock and severe spillage. In contrast, the chevron-modified intake maintains an attached oblique-shock system and prevents choking, demons–trating a significantly expanded operability margin and improved robustness during off-design excursions.

Three-dimensional simulations confirmed the forma–tion of stable counter-rotating vortex pairs (CVP) and validated the accuracy of the 2D parametric optimization, showing consistent trends in flow attach–ment, TPR enhancement, and bubble suppression.

Overall, this work establishes that carefully dimen–sioned chevron grooves provide a simple, lightweight, and passive method to suppress SBLI, improve pres–sure recovery, reduce distortion, and delay unstart in high-speed intakes. Future work should explore experimental validation, extension to variable-geo–metry inlets, and hybrid passive–active control strate–gies to further advance intake operability across vary–ing Mach conditions.

ACKNOWLEDGMENTS:

Authors are thankful to Amity University Uttar Pradesh for providing their support in conducting the research work.

REFERENCES

[1] Soltani MR et al.: Performance investigation of a supersonic air intake in the presence of the boun–dary layer suction. Proceedings of the Institution of Mechanical Engineers, Part G: Journal of Aerospace Enginee–ring 2015;229:1495–509.

[2] Koval SN.: Optimization of the Supersonic Engine Inlet 2020:32–6.

[3] Gahlot NK, Singh NK.: Parametric Study on Inf–luence of an Array of Air Jets on the Performance

of Supersonic Air Intake by Varying the Jet Injection and Back Pressure. Journal of Aerospace Engineering 2021;34:04021086.

[4] Dolling DS.: Fifty Years of Shock-Wave/ Boundary-Layer Interaction Research: What Next? AIAA Journal 2001;39:1517–31.

[5] Abbas A, De Vicente J, Valero E.: Aerodynamic technologies to improve aircraft performance. Ae–rospace Science and Technology 2013;28:100–32.

[6] Gahlot NK, Singh NK. Starting Characteristic of Supersonic Mixed Compression Air Intake with Cowl Porosity.: Journal of Physics: Conference Series, vol. 1240, 2019.

[7] Gahlot NK, Singh NK.: Flow Field Study of Mixed Compression Supersonic Air Intake with Cowl Ventilation. Journal of Applied Fluid Mechanics 2020;13:1795–805.

[8] Loginov MS, Adams NA, Zheltovodov AA.: Large -eddy simulation of shock-wave/turbulent-boundary-layer interaction. J Fluid Mech 2006;565:135–69.

[9] E. Garnier, N. A. Adams, P. Sagaut Large Eddy Simulation for Compressible Flows. Springer, 2009.

[10] Pasquariello V, Grilli M, Hickel S, Adams NA.: Large-eddy simulation of passive shock-wave/ boundary-layer interaction control. Int J Heat Fluid Flow 2014;49:116–27.

[11] Koo H, Raman V.: Large-eddy simulation of a supersonic inlet-isolator. AIAA Journal 2012;50: 1596–613.

[12] Debonis JR, Oberkampf WL, Wolf RT, Orkwis PD, Turner MG, Babinsky H.: Assessment of Computational Fluid Dynamics (CFD) Models for Shock Boundary-Layer Interaction. 2011.

[13] Sinha J, Singh S, Prakash O, Panchal D.: Passive Flow Modification Over the Supersonic and the Hypersonic Air-Intake System Using Bleed. FME Transactions 2023;51:329–37.

[14] Tarakka R, Salam N, Jalaluddin, Ihsan M.: Effect of blowing flow control and front geometry towards the reduction of aerodynamic drag on vehicle models. FME Transactions 2019;47:552–9.

[15] Babinsky H, Ogawa H.: SBLI control for wings and inlets. Shock Waves 2008;18:89–96.

[16] Kumar V V, Bogadi S.: Effect of Micro-Vortex Generator in Hypersonic Inlet 2011:10–3.

[17] Sabnis K, Babinsky H.: A review of three-dimen–sional shock wave–boundary-layer interactions. Progress in Aerospace Sciences 2023;143:100953.

[18] Grébert A, Bodart J, Jamme S, Joly L.: Simula–tions of shock wave/turbulent boundary layer interaction with upstream micro vortex generators. International Journal of Heat and Fluid Flow 2018;72:73–85.

[19] Babinsky H, Li Y, Pitt Ford CW.: Microramp Control of Supersonic Oblique Shock-Wave/ Boundary-Layer Interactions. AIAA Journal 2009;47:668–75.

[20] Panaras AG, Lu FK.: Micro-vortex generators for shock wave/boundary layer interactions. Progress in Aerospace Sciences 2015;74:16–47.

[21] Zhang Y, Tan H, Tian F-C, Zhuang Y.: Control of Incident Shock/Boundary-Layer Interaction by a Two-Dimensional Bump. AIAA Journal 2014;52:767–76.

[22] Lv Y, Li Q, Li S.: Modeling the Effect of Stability Bleed on Back-Pressure in Mixed-Compression Supersonic Inlets. Journal of Fluids Engineering, Transactions of the ASME 2015;137:1–13.

[23] Das S & JKP, Prasad JK.: Starting characteristics of a rectangular supersonic air-intake with cowl deflection. Aeronautical Journal 2010;114:177–89.

[24] Bajaj DK, Kansara ST, Nath NK, Vashishtha A, Sahoo D.: Enhancement of scramjet inlet effici–ency by geometrical modifications. Advances in Aerodynamics 2025;7.

[25] Soltani MR, Daliri A, Younsi JS, Farahani M.: Effects of bleed position on the stability of a supersonic inlet. Journal of Propulsion and Power 2016;32:1153–66.

[26] Giehler J, Leudiere T, Morgadinho RS, Grenson P, Bur R.: Experimental and numerical investigation of porous bleed control for supersonic/subsonic flows, and shock-wave/boundary-layer interactions. Aerospace Science and Technology 2024;147.

[27] Khobragade N, Kumar R.: Control of shock wave/ boundary layer interactions in a supersonic air intake using a modified backward-facing step. Shock Waves 2022;32:467–83.

[28] Vijay A, Agarwal P, Dsouza LF, AJ U, Naveen K, Jha AK, Singh N, Saluja RK, Gahlot NK.: Nume–rical investigation of shock wave boundary layer interaction management in supersonic duct with repeated backward facing steps configuration. Proceedings of the Institution of Mechanical Engi–neers, Part G: Journal of Aerospace Engineering 2025;0:1–14.

[29] Emami S, Trexler CA, Auslender AH, Weidner JP.: Experimental investigation of inlet-combustor isolators for a dual-mode scramjet at a Mach number of 4. NASA Technical Paper 3502 1995.

[30] Bridges J, Brown CA.: Parametric Testing of Chevrons on Single Flow Hot Jets. 2004.

[31] Lin JC.: Review of research on low-profile vortex generators to control boundary-layer separation. vol. 38. 2002.

[32] Babinsky H, Makinson N, Morgan C.: Micro-Vortex Generator Flow Control for Supersonic Engine Inlets. 45th AIAA Aerospace Sciences Meeting and Exhibit 2007:2007.

[33] Coratekin T, Van Keuk J, Ballmann J.: Prelimi–nary investigations in 2D and 3D ramjet inlet design. 35th Joint Propulsion Conference and Exhibit 1999:1–11.

[34] DeBonis JR, Oberkampf WL, Wolf RT, Orkwis PD, Turner MG, Babinsky H, Benek JA.: Assess–

ment of computational fluid dynamics and experimental data for shock boundary-layer interactions. AIAA Journal 2012;50:891–903.

[35] Saha S, Chakraborty D.: Hypersonic intake starting characteristics-A CFD validation study. Defence Science Journal 2012;62:147–52.

[36] Gahlot NK, Singh NK.: Effect of air jet with injection pressure on the performance of mixed compression air intake. Proceedings of the Institution of Mechanical Engineers, Part G: Journal of Aerospace Engineering 2021;235:1105–17.

[37] \Settles GS, Dodson LJ.: Supersonic and hypersonic shock/boundary-layer interaction database. AIAA Journal 1994;32:1377–83.

[38] Vuković D, Damljanović D, Ocokoljić G, Ilić B.: Application of a technique for reducing supersonic starting loads on internal wind tunnel balances. Advances in Mechanical Engineering 2022;14:1–15.

[39] Askari R, Solani MR.: Effects of Mach number on the performance of a diverterless supersonic inlet. Journal of Aircraft 2019;56:1697–707.

[40] Sepahi-Younsi J, Forouzi Feshalami B.: Performance Evaluation of External and Mixed Compression Supersonic Air Intakes: Parametric Study. Journal of Aerospace Engineering 2019;32:1–14.

[41] Grébert A, Bodart J, Jamme S, Joly L.: Simulations of shock wave/turbulent boundary layer interaction with upstream micro vortex generators. International Journal of Heat and Fluid Flow 2018;72:73–85.

NOMENCLATURE

f	Frequency of chevron
H	Height of throat
h	Depth of chevron grooves
L	Length of model
M	Mach Number
P	Static pressure
P_t	Total pressure
w	Width of chevron grooves

Acronyms

CFD	Computational Fluid Dynamics
CGM	Chevron Groove Modification
CVP	Counter-rotating Vortex Pairs
DC	Distortion Coefficient
LES	Large Eddy Simulation
MCR	Mass Capture Ratio
RANS	Reynolds-Averaged Navier-Stokes
SBLI	Shock-wave Boundary Layer Interaction
SF	Separation Factor
SST	Shear Stress Transport
TPR	Total pressure recovery

Subscripts

min	Minimum
avg	Average
exit	Exit of intake
sep	Separation
inf	Freestream conditions
max	Maximum
min	Minimum

Greek symbols

α	Ramp angle
δ	Boundary layer hight

ПАСИВНА КОНТРОЛА ПРОТОКА УСИСНИКА СА МЕШОВИТОМ КОМПРЕСИЈОМ МАХА 4 ПОМОЋУ ЖЛЕБОВА ШЕВРОНА

Ј.А. Гуџар, Ш. Тјаги, А.С. Мехбуб, Н. Сингх, Р.К. Салуџа, М. Нагар, Н.К. Галот

Ефикасан рад надзвучних усисника често је отежан интеракцијом ударног удара и граничног слоја (SBLI), која изазива велике мехуриће одвајања, губитке притиска и неуједначен проток на челу мотора. Да би се решили ови изазови, овај рад представља модификације жлебова шеврона (CGM) као нову стратегију пасивне контроле протока. Моделиран је дводимензионални усисник са мешовитом компресијом Маха 4, а три конфигурације жлебова, надоле, средња површина и нагоре, имплементиране су на површини рампе близу подножја ударног удара. Симулације високе резолуције Рејнолдс-усредњеног Навије-Стоксовог (RANS) модела са k–ω SST моделом су извршене како би се проценили ефекти на фактор одвајања (SF), опоравак укупног притиска (TPR) и коефицијент дисторзије (DC). Резултати показују да су жлебови шеврона усмерени нагоре (Случај U-1) обезбедили најефикаснију контролу, смањујући мехурић одвајања грла за приближно 83%, смањујући дисторзију за ~30% и побољшавајући TPR у поређењу са основним случајем. Даља параметарска истраживања дубине и фреквенције жлебова открила су да плитки, високофреквентни жлебови (Случај U-1B: дубина 1 mm, фреквенција = 8) постижу најбољи баланс, дајући глатке расподеле притиска, ниске вредности коефицијента дејства енергије (SF) и дисторзију смањену на 38,8%. Ова побољшања се приписују стварању јаких супротно ротирајућих вртлога, који поново енергизују гранични слој и слабе неповољне интеракције ударних таласа. Додатне тродимензионалне симулације потврђују поузданост 2D предвиђања и хватају ефекте по распону. Ванпројектне анализе у распону од 2,5 до 4,0 Маха показују да CGM побољшава робусност усиса, одржавајући стабилан надзвучни ток, уз занемарљиве казне за отпор. Ови налази утврђују шевронске жлебове као ефикасну, геометријски засновану технику пасивне контроле за побољшање стабилности, опоравка притиска и оперативности у системима погона који дисају ваздух велике брзине.

Received: October 2025, Accepted: Decembar 2025
Correspondence to: Neeraj Kumar Ghalot, Amity Institute of Aerospace Engineering (AIAE), Amity University Uttar Pardesh, Noida, India
E-mail: neerajkumargahlot@gmail.com
doi: 10.5937/fme2601053G